Electronic Supplementary Material (ESI) for Physical Chemistry Chemical Physics.

Supplemental material for

Structure and energetics of liquid water-hydroxyl layers on Pt(111)

August E. G. Mikkelsen[1], Henrik H. Kristoffersen[2], Jakob Schiøtz[3], Tejs Vegge[1], Heine A. Hansen and Karsten W. Jacobsen[3]
[1] *Department of Energy Conversion and Storage, Department of Physics, Technical University of Denmark, DK-2800 Kgs. Lyngby, Denmark*
[2] *Department of Chemistry, University of Copenhagen, Copenhagen 2100, Denmark and*
[3] *CAMD, Department of Physics, Technical University of Denmark, DK-2800 Kgs. Lyngby, Denmark*
(Dated: February 21, 2022)

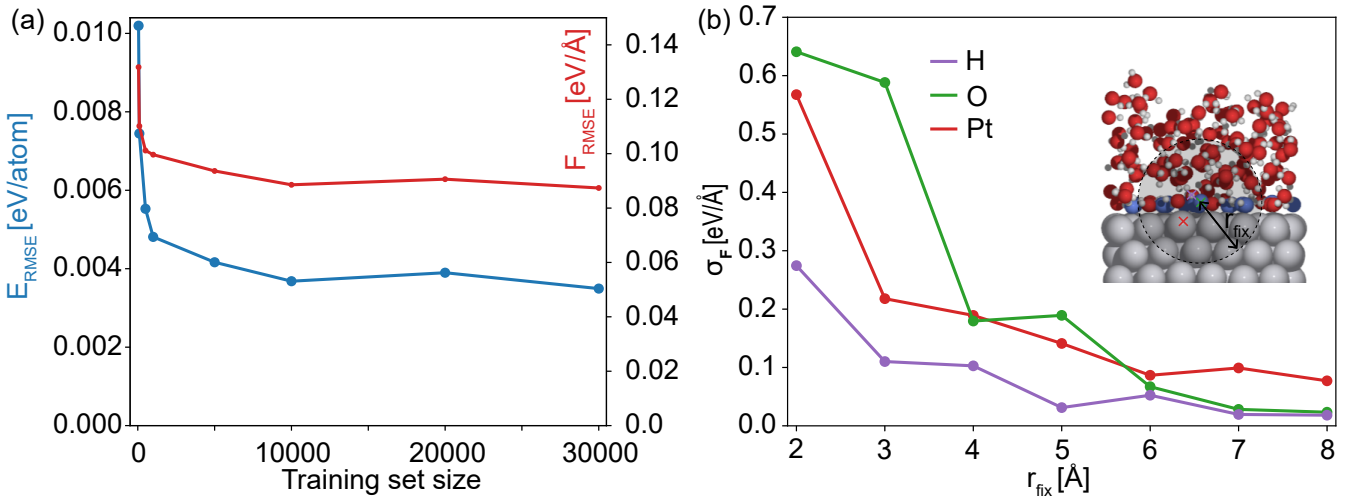

FIG. 1. (a) Learning curve displaying the error in the energies (blue line) and forces (red line) on a fixed test set as the training set is systematically expanded. (b) A measure of the locality of the water-OH/Pt(111) interface based on the procedure of Deringer and Csányi [2]. In the inset hydroxyls are colored blue, and the fixed O and H atom were chosen to belong to one of these.

A. Model and data set limitations

Similar to the our previous study of the water/Pt(111) interface [1], we have analyzed the significance of long-range interactions and dataset limitations for our system using learning curves and the locality estimate suggested by Deringer and Csányi [2].

The learning curve was determined by setting aside a fixed test set of 71 377 structures chosen randomly from our database, and then incrementally expanding the training set using the remaining ones, while monitoring the error on the forces and energies. As shown in Fig. 1 (a) the error in the forces and energies on the fixed test set drops rapidly as a function of training set size up to around only $\sim$ 100 structures after which the improvement is much more modest. This is similar to what was observed for the water/Pt(111) interface [1], though the decay is more gradual indicating that a larger number of chemically different structures are needed to accurately describe the energetics of the interface with hydroxyls present. The saturation values are also larger than those of reported in [1]. Finally, we note that while the learning curve in Fig. 1 (a) appears to suggest, that we could have done equally well with NNPs trained on much smaller training sets, this is in practice not true as the latter would give rise to instabilities during the NNP-based MD simulations. In fact, even with as large a training set as the one employed here, some of the trained NNPs still led to unstable MD simulations for certain OH coverages, where the atoms would drift into unreasonable parts of configuration space.

In the locality test proposed by Deringer and Csányi [2], a central atom is chosen and every atom within a distance of r_{fix} are then fixed while atoms outside are distorted randomly. By then monitoring the standard deviation of the force on the central atom, an estimate of the locality of the system is obtained. In our case we focused on the O, H and Pt atoms shown in Fig. 1 (b) and performed calculations in a $2 \times 2 \times 1$ unit cell compared to the computational cell of the training structures ($1 \times 1 \times 1$ k-points were used for consistency) to be able to investigate values of r_{fix} up to 8. Compared to the results of [1] the long-range character is more pronounced with the presence of hydroxyls at the interface, as reflected in the slower decay of the force standard deviation and the fact that the curves saturate at values as large as $\sim$ 0.1eV/. A plausible explanation for this more long-ranged behaviour could be that the interaction between co-adsorbed water and OH molecules is known to be of mainly electrostatic origin [3]. We also note that the observation of a more long-ranged character, ties well with our previous comment of the higher training and test errors of our NNPs compared to those reported in [1].

B. Obtaining accurately sampled internal energies

For every NNP in our ensemble the internal energy averages corresponding to the different OH coverages in (3) of the main paper were determined from three 10ns MD simulations started from different structures. The average internal energy obtained from each of these runs are reported in Tables I, II, III, IV, where it is clear that we obtain averages which agree within $\sim$ 0.025eV for runs started from different points in phase space. To obtain the final values employed in (3) of the main paper the averages corresponding to each coverage and NNP were averaged over the three independent runs.

n_{OH}	θ_{OH}	$\langle E_{(n_{\mathrm{H_2O}}-n_{\mathrm{OH}})\cdot \mathrm{H_2O}+n_{\mathrm{OH}}\cdot \mathrm{OH}}\rangle$ [eV]
0	0.0	-2849.90, -2849.91, -2849.92
4	0.083	-2833.35, -2833.37, -2833.37
8	0.167	-2816.73, -2816.75, -2816.74
12	0.250	-2800.15, -2800.14, -2800.15
16	0.333	-2783.50, -2783.53, -2783.54
20	0.417	-2766.83, -2766.79, -2766.83
24	0.500	-2749.71, -2749.73, -2749.71
28	0.583	-2732.04, -2732.02, -2732.04
32	0.667	-2713.75, -2713.77, -2713.75
36	0.750	N/A
40	0.833	N/A

TABLE I. Average internal energies corresponding to different coverages and MD runs as predicted by NNP1. Values from the last two rows are absent as the NNP-based MD simulations were unstable for these two coverages.

n_{OH}	θ_{OH}	$\langle E_{(n_{\mathrm{H_2O}}-n_{\mathrm{OH}})\cdot \mathrm{H_2O}+n_{\mathrm{OH}}\cdot \mathrm{OH}}\rangle$ [eV]
0	0.0	-2849.69, -2849.69, -2849.69
4	0.083	-2833.15, -2833.17, -2833.17
8	0.167	-2816.60, -2816.62, -2816.58
12	0.250	-2800.05, -2800.02, -2800.07
16	0.333	-2783.47, -2783.46, -2783.48
20	0.417	-2766.82, -2766.81, -2766.85
24	0.500	-2749.76, -2749.80, -2749.78
28	0.583	-2732.09, -2732.04, -2732.14
32	0.667	-2713.75, -2713.71, -2713.81
36	0.750	-2694.95, -2694.92, -2694.96
40	0.833	-2674.97, -2674.96, -2674.96

TABLE II. Average internal energies corresponding to different coverages and MD runs as predicted by NNP2.

n_{OH}	θ_{OH}	$\langle E_{(n_{\mathrm{H_2O}}-n_{\mathrm{OH}})\cdot \mathrm{H_2O}+n_{\mathrm{OH}}\cdot \mathrm{OH}} \rangle$ [eV]
0	0.0	-2849.69, -2849.69, -2849.66
4	0.083	-2833.23, -2833.22, -2833.22
8	0.167	-2816.70, -2816.67, -2816.67
12	0.250	-2800.15, -2800.13, -2800.13
16	0.333	-2783.55, -2783.54, -2783.57
20	0.417	-2766.90, -2766.86, -2766.87
24	0.500	-2749.77, -2749.81, -2749.81
28	0.583	-2732.14, -2732.07, -2732.09
32	0.667	-2713.79, -2713.82, -2713.84
36	0.750	-2694.98, -2695.00, -2695.16
40	0.833	-2675.27, -2674.29, -2674.28

TABLE III. Average internal energies corresponding to different coverages and MD runs as predicted by NNP3.

n_{OH}	θ_{OH}	$\langle E_{(n_{\mathrm{H_2O}}-n_{\mathrm{OH}})\cdot \mathrm{H_2O}+n_{\mathrm{OH}}\cdot \mathrm{OH}} \rangle$ [eV]
0	0.0	-2849.88, -2849.87, -2849.87
4	0.083	-2833.35, -2833.37, -2833.38
8	0.167	-2816.76, -2816.74, -2816.78
12	0.250	-2800.16, -2800.12, -2800.13
16	0.333	-2783.53, -2783.48, -2783.51
20	0.417	-2766.88, -2766.83, -2766.89
24	0.500	-2749.84, -2749.81, -2749.83
28	0.583	-2732.11, -2732.14, -2732.10
32	0.667	-2713.80, -2713.74, -2713.75
36	0.750	-2694.98, -2694.91, -2694.90
40	0.833	N/A

TABLE IV. Average internal energies corresponding to different coverages and MD runs as predicted by NNP4. Values from the last row are absent as the NNP-based MD simulations were unstable for this coverage.

[1] A. E. G. Mikkelsen, J. Schiøtz, T. Vegge, and K. W. Jacobsen, The Journal of Chemical Physics **155**, 224701 (2021).
[2] V. L. Deringer and G. Csányi, Phys. Rev. B **95**, 094203 (2017).
[3] G. S. Karlberg and G. Wahnström, The Journal of Chemical Physics **122**, 194705 (2005).